Surface modifications to reduce wear in hot extrusion of copper

Alexander Thewes [a,b,*], Phillip Marvin Reinders [a,b], Hanno Paschke [b], Tristan Brückner [b], Daniel Templin [b], Stefan Lechner [c], Sören Müller [c], Michael Paulus [d], Christian Sternemann [d]

[a] *Institute for Surface Technology, TU Braunschweig, Riedenkamp 2, 38108 Braunschweig, Germany*
[b] *Fraunhofer Institute for Surface Engineering and Thin Films IST, IST at DOC, Eberhardstr. 12, D-44145 Dortmund, Germany*
[c] *Extrusion Research & Development Center, TU Berlin, Gustav-Meyer-Allee 25, Building 17a, Stair 5, D-13355 Berlin, Germany*
[d] *Fakultät Physik/DELTA, TU Dortmund, Maria-Goeppert-Mayer-Straße 2, D-44227 Dortmund, Germany*

A B S T R A C T

During hot extrusion of copper, the material tends to stick to the extrusion die due to strong adhesive forces between hot working steel and copper at high temperatures. In this context, surface modifications like nanocomposite coatings deposited by plasma enhanced chemical vapor deposition or boriding of nickel-based alloy 718 (DIN 2.4668) create hard and wear resistant thin solid films that offer high temperature stability. Ti–Si–B–C–N nanocomposite coatings consist of nanocrystalline grains embedded in a thin amorphous matrix. Due to this particular nanostructure, hardness values of up to 39.3 GPa were reached. Boriding of alloy 718 leads to formation of phases consisting of alloying elements like nickel, iron, and chromium and the diffusing element boron. The borides form a boriding zone that offers high hardness. Extrusion of Ø122 mm × 300 mm copper billets preheated to 850 °C was carried out and adhesive wear on tool's surfaces was analyzed. The comparison between hot working steel DIN 1.2367 without surface modification and with Ti–Si–B–C–N coating or borided alloy 718 showed remarkable differences between conventional tools made of hot working steels/alloy 718 and tools with surface modification. A strong decrease particle adhesion was observed.

1. Introduction

The increase of production in hot extrusion of copper is mandatory for society's transition from combustion to electric engines in automotive mobility [1]. Copper strings are crucial for manufacturing power cables inside cars, electric engines, and recharging infrastructure for batteries. Increasing tool lifetime of extrusion dies is one way to lower production costs and improve the ecological balance of the process. Adhesive wear between hot copper and tool's surface is a major mechanism that accelerates wear on extrusion dies.

To reduce adhesive wear, two different surface properties of the tools are required: First, the surface needs to be thermally stable, as hot extrusion of copper is carried out at temperatures up to 1000 °C. Second, a chemical state close to inertness is beneficial to minimize the interaction between hot copper and the tool's surface. The general approach within this study is to form boron containing hard phases at the tool's surface either formed from nickel, iron, and chromium borides in alloy 718 nickel superalloy or by forming a nanocomposite coating with nanocrystalline (nc)-/amorphous(a)-TiB$_2$, a-BN, and a-B$_4$C incorporated

in the nanostructure [2–6]. Thus, boriding of alloy 718 is carried out and a coating is applied by plasma enhanced chemical vapor deposition (PECVD) on hot working steel DIN 1.2367. Powder pack or gas boriding of pure nickel [7] and nickel-based alloys like Nimonic 90 [8], alloy 600 [9,10], and alloy 718 [11–13] lead to an increase in surface hardness and promising tribological properties. Preliminary studies by the authors on Ti–Si–B–C–N nanocomposite coatings offered hot forming as a possible field of application [14].

2. Experimental details

Extrusion die inserts with an outer diameter of Ø50 mm and a die angle of 150° were made of hot working steel DIN 1.2367 and solution annealed nickel-based alloy 718 (DIN 2.4668). The bearing channel diameter and length, as well as the lead-in radius were 14 mm, 10 mm, and 3 mm, respectively. Before the surface treatments were carried out, the tools and shims were hand cleaned using tissues and isopropyl alcohol and subsequently ultrasonically cleaned in isopropyl alcohol for 15 min.

2.1. Surface modifications

Gas boriding of alloy 718 was carried out in a PlaTeG PP20 device (PVA TePla AG, Germany) at 700 Pa. Precipitation hardening of substrate material is carried out simultaneously by following an industrially common heat treatment routine of heating up to 720 °C and holding the temperature for 8 h, then reducing the temperature with 55 °C/h to 620 °C and holding the temperature again for 8 h. The boriding step was incorporated in the first holding step at 720 °C by changing the gaseous atmosphere from H_2 to a mixture of N_2 (870 sccm), H_2 (1000 sccm), and BCl_3 (50 sccm) for the last 4 h. H_2 is used to reduce BCl_3 to solid and diffusible B and HCl waste, whereas N_2 is applied to increase kinetic activity within the atmosphere due to its heaviness compared to H_2 and inertness in the process.

Furthermore, in a second approach PECVD was used to form a thin solid nanocomposite film of Ti–Si–B–C–N. The process was carried out on the die inserts as well as on single crystalline Si wafers (*ca.* $10 \times 10 \times 0.2$ mm^3) for coating characterization. A PN 100/150 device (Ruebig GmbH & Co. KG, Austria; see Ref. [15]) was used to perform a plasma etching routine, carry out a plasma-nitriding process, and synthesize the coating. Plasma etching was performed for 1 h whereas plasma nitriding was carried out for 8 h in an atmosphere with low $N_2/(N_2+H_2)$ ratio of 5% and additional Ar for plasma support. Furthermore, the pressure, the applied bias voltage, and the substrate temperature were 240 Pa, −450 V, and 530 °C, respectively. Plasma nitriding was utilized to increase the adhesion between the steel substrate and hard coating, as noticed in other works [16,17]. The PECVD coatings consist of an adhesion layer of TiN, a graded interlayer and a top layer of Ti–Si–B–C–N. For top layer deposition of samples under HR-TEM (high-resolution transmission electron microscopy) investigation, the pressure was set to 200 Pa and N_2 flow to 333 sccm, whereas for coating synthesis on extrusion die inserts 300 Pa and 667 sccm N_2 were used. The other parameters were identical in both cases. The following precursor were used to synthesize the top layer: $TiCl_4$ (77 sccm), N_2 (333/667 sccm), BCl_3 (200 sccm), Tetramethylsilan (67 sccm), H_2 (3333 sccm), and Ar (100 sccm). The bias voltage was −560 V and the duty cycle 0.33. The substrate temperature was held at 530 °C, as it has been during nitriding.

2.2. Analytical procedures

There are major differences between thermochemical surface treatments and coating depositions, making different means of characterization necessary for each process. The characterization was performed on shims of Ø34 mm × 4 mm or single crystalline Si-wafers.

In the following, the characterization of borided alloy 718 is described. The thickness of the borided zone was determined using a kaloMAX NT device (BAQ GmbH, Germany), as described by Leroy et al. [18] and measurement in cross-sectional view. A Daimler-Benz-test was performed to classify the adhesion of the borided compound layer to the substrate material. The phase composition of the samples was characterized by X-ray diffraction. The measurements were performed at beamline BL9 of the synchrotron radiation source DELTA (TU Dortmund, Dortmund, Germany) [14,19]. The X-ray energy was 13 keV and the angle of incidence was set to 1° at a beamsize of 0.2×1.5 mm^2 (v x h). Diffraction patterns were measured at room-temperature by scanning a Pilatus 100 K (Dectris, Baden-Daettwil, Switzerland) detector. The roughness was determined with a Hommel Tester T1000 (Hommel + Seitz GmbH, Germany) by dragging a stylus across the surface and plotting the tip deflection. R_t and R_a values were calculated according to DIN EN ISO 4287. The hardness of the substrate material was measured by HRC tests before and after the surface modification, as simultaneously precipitation hardening was carried out and an increase in hardness should be observed. The hardness of the borided zone and its Young's modulus were determined by indentation in cross-section with a Fischerscope device (Fischer, Germany), as vertical indentations into the surface yielded no consistent results. 17 indentations in accordance with DIN EN ISO 14577 were carried out with huge variation towards lower hardness due to challenges in measurement, so that the highest five values are presented. Oxidation resistance was analyzed by annealing the samples in air at 850 °C for 30 min and preparing a cross-sectional image to take a look at the borided zone, substrate material, and potential oxide layer.

The procedure for Ti–Si–B–C–N PECVD nanocomposite coatings is different from borided samples. Its chemical composition is determined by means of electron probe microanalysis (EPMA) under use of an electron probe microanalyzer SX100 device (Cameca, France). The time between coating deposition und EPMA measurement was twelve months and oxidation and degradation of the surface had taken place. So, the absolute values for the elements are not available, but ratios between the coating elements. The excitation energy in EPMA measurements was set to 10 keV and five measurements per sample were carried out. The thickness of the coating was determined by calotest (same as borided samples), whereas the nanocomposite structure was investigated by TEM as well as by X-ray diffraction analysis. The diffraction experiments were performed at beamline BL9 as described for borided samples. In addition, the samples were annealed in air for *in-situ* X-ray diffraction measurements utilizing an Anton Paar DHS1100 (Anton Paar, Graz, Austria) cell equipped with a graphite dome. The roughness was characterized as described for borided samples and the hardness was determined with a Fischerscope device (Fischer, Germany) performing eleven indentations (DIN EN ISO 14577) removing the oxide top-layer by dry-polishing with a DryLyte device (GPAINNOVA, Spain). To evaluate oxidation resistance, annealing in air was carried out at 850 °C for 30 min. The thickness of the oxidized and unoxidized coating was determined by calotest method and optical appearance was taken into account, e.g. a crack network or coloring of top-layer.

2.3. Hot extrusion trials

The hot extrusion trials were performed on the 8 MN extrusion press (SMS Schloemann AG, Germany) of the Extrusion Research and Development Center (TU Berlin, Germany). A modular 2-hole die with inserts was used as a tool. For the two extrusion trials, one pair each of the inserts described in section 2 was applied. Moreover, an untreated reference insert and a surface-modified insert made of the same tool material (DIN 1.2367 or alloy 718) were paired for each extrusion. In order to emphasize the effects of adhesion between the billet material (Cu-DHP) and the tool materials, lubrication of the die and insert faces was omitted. All relevant extrusion parameters are listed in Table 1.

2.4. Wear analysis on copper extrusion dies

After extrusion, the die inserts were extracted and analyzed with respect to adhesive wear. Other wear mechanisms are abrasive wear, tribo-corrosion, and surface fatigue. Copper itself is a soft metal and even more so at elevated temperatures, thus in contact with hard surface modifications (hardness >1.500 $HV_{0.005}$), the abrasive wear is neglectable. Tribo-corrosion is also neglectable because of the very short processes of several seconds and the exclusion of air from the extrusion process. With a homogenous flow of copper over the surface of the extrusion die and the low roughness of the extrusion die, surface fatigue is also of no consequence to the hot extrusion process. For evaluation of

Table 1
Relevant parameters of the direct extrusion trials.

Container diameter	Profile diameter	Extrusion ratio	Ram speed
125 mm	2 × 14 mm	40 : 1	15 mm/s
Container/Tool Temperature	**Billet dimensions**	**Billet temperature**	
500 °C	Ø122 × 300 mm	850 °C	

adhesive wear, photographs of the die faces were taken and subsequently processed using the freeware GNU Image Manipulation Program (GIMP). A digital image analysis was performed utilizing the particle analysis algorithm of the freeware ImageJ and the area covered with copper was determined. Another aspect of this tribological system is the friction factor. The authors investigated this for untreated DIN 1.2367, Ti–Si–B–*C*–N coated DIN 1.2367, and borided Alloy 718 b y using an axial friction-tester device and published the set-up and results in Lechner et al. [20]. The main finding of that study was, that a significant decrease in friction was observed for the amorphous-carbon (a-C) containing Ti–Si–B–*C*–N coating, whereas the friction factor of untreated DIN 1.2367 and borided Alloy 718 are in the same range.

3. Results and discussion

The borided alloy 718 showed a thickness of 7 μm. Only minor radial cracks appear around the indentation crater, making it adhesion class HF2 (see Fig. 1 a.). The X-ray diffraction pattern of borided Alloy 718 is given in Fig. 2. Ni_2B is the phase that is identified in nine characteristic reflexes. This agrees with the results published by Ueda et al. [7] and Lou et al. [8] for powder pack borided 99.9% pure Ni samples. Additionally, (200) Ni_4B_3 is identified. Alloy 718 consists of ~55% Ni, ~19% Fe and ~18% Cr. Two major alloying elements of Alloy 718 are Cr (~18%) and Fe (19%). There are no Cr_xB reflexes observed, as the boriding temperature was only 720 °C, but >850 °C is required to form Cr_xB instead of Ni_xB. Fe_xB reflexes often match those of Ni_xB reflexes and are often indistinguishable from one another (compare X-ray diffraction patterns of Campos-Silva et al. [12]). It can only be assumed, that Fe_2B and/or FeB is formed, but regardless, the borided compound layer is mainly composed of Ni_2B. The surface roughness R_t and R_a were 1.14 ± 0.43 μm and 0.092 ± 0.007 μm, respectively. The R_t value is the vertical difference between the maximum profile peak and maximum valley depth and should not be above 3 μm for extrusion dies. The arithmetical mean height R_a is the average of the absolute values along the sampling length and should be below 0.5 μm. Both values for R_t and R_a are in accordance with these commonly used threshold values. The hardness of the substrate material was 250 H V before the process and 434 H V after. The hardness of the borided zone was 1623 ± 136 $HV_{0.005}$ and Young's modulus was 215 ± 11 GPa. The hardness shows significant variation due to the thin borided zones in the cross-section (7 μm) adjacent to soft phases like precipitation hardened alloy 718 and embedding compound. After annealing in air for 30 min at 850 °C, no oxide layer is detected in cross-sectional view and both, the boron rich diffusion zone and the boride compound layer are clearly visible and intact (see Fig. 2). A top view image is given at the bottom right in Fig. 2, with no indication of damage caused by oxidation (see Fig. 3).
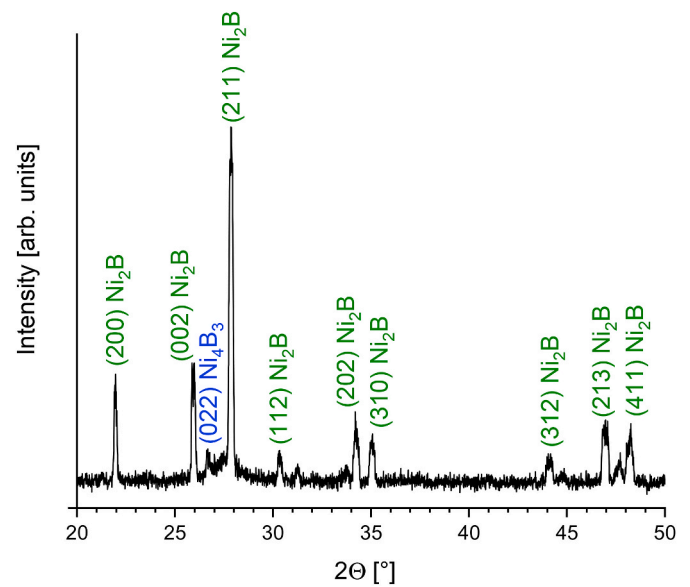

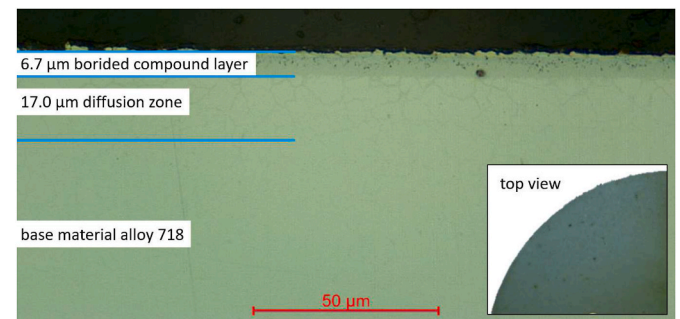**Fig. 2.** X-ray diffraction pattern of gas borided Alloy 718.

Fig. 3. Cross-sectional view of an air annealed borided alloy 718 sample.

Proving the nanocomposite structure of Ti–Si–B–*C*–N coatings is challenging, as nc-grains and the a-matrix can only be identified with nanoanalytics. This was carried out on samples from a similar process with minor differences in deposition conditions as described before and presumably only a slightly different chemical composition. EPMA results yielded no valid results for coated Si-wafer samples from the tool coating process, as degradation and oxidation of the coating due to one
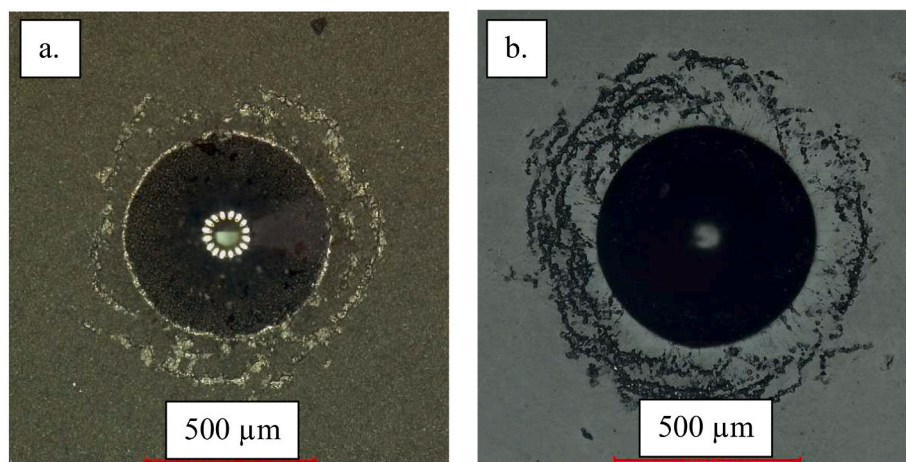

Fig. 1. HRC indent of a. Borided alloy 718 and b. Ti–Si–B–*C*–N coated 1.2367.

year of aging in air resulted in an oxygen content of 19.0 at.-%. The stoichiometry of samples used for HR-TEM investigations and X-ray diffration experiments was 30.0 at.-% Ti, 9.6 at.-% Si, 15.5 at.-% B, 32.0 at.-% C, 8.7 at.-% N, 1.5 at.-% O, and 2.7 at.-% Cl. HR-TEM images are presented in Fig. 4 and show a nanocomposite structure, as the orientation of grains varies within a few nanometers as indicated by blue lines. Analysis of the X-ray diffraction measurement of this sample at room temperature yields a grain size of approximately 6 nm applying the Scherrer equation with a shape factor K of 0.9 to the (200) Ti(C,N) diffraction peak, in good agreement with the results of HR-TEM. Patscheider et al. [21] state, that the grain size in such nanocomposite coatings should be between 3 and 10 nm. Pilloud et al. [22] calculated the grain size of Ti–Si–N coatings to 10 nm using Scherrer equation. Mayrhofer et al. [23] measured grain sizes of 2–3 nm in HR-TEM images.

Nanocomposite Ti–Si–B–*C*–N coatings can differ significantly in chemical composition, hardness and nanostructure. The PECVD coatings were 2.5 µm thick and showed adhesion class HF2, due to minor radial cracks around the HRC indent (see Fig. 1 b.). The surface roughness R_t and R_a were 0.66 ± 0.40 µm and 0.043 ± 0.021 µm, respectively. The smoothness of the coatings makes a grinding or polishing routine after coating deposition obsolete. The hardness was 1559 ± 172 $HV_{0.005}$ with a Young's modulus of 189 ± 12 GPa. The sample's hardness and Young's modulus were measured one year after the deposition process, with an oxide layer on the surface. The oxide layer and presumably parts of the coatings were removed with dry-polishing. This made it possible to circumvent the influence of an oxide layer, but lead to additional decrease in coating thickness and made measurements more difficult.

Fig. 5 shows a crater created by ball cratering method on a tempered sample (Ti–Si–*C*–N, 850 °C, 30 min, air). The overview on the righthand side suggests oxidation, as these coatings form an almost pure TiO_2 layer of several dozen nanometers, resulting in tempering colors. Investigating the crater shows, that only a minor amount of the coating is affected by oxidation, whereas the major part is still in as-deposited condition. A fine mesh of cracks was identified in close-up view, but the crater indicates no significant increase in oxidation progress by these cracks. This leads to the conclusion, that oxidation is slowly progressing at temperatures relevant for hot extrusion of copper. *In-situ* X-ray diffraction experiments at elevated temperatures showed a minor decrease in (200) Ti(C,N) diffraction peak intensity while between 800 °C and 850 °C crystalline rutile ((110) and (211) reflections) and anatase ((112) and (200) reflections) TiO_2 phases form with increasing intensity from 850 °C to 875 °C (see Fig. 6). The (200) Ti(C,N) diffraction peak measured at an annealing temperature of 875 °C is still significantly stronger than the TiO_2 reflexes, indicating a thin oxidized top-layer with an as-deposited Ti–Si–B–*C*–N coating underneath. These results agree with the analysis presented in Fig. 5. In the following, the focus is on the samples of the hot extrusion trials which have not been studied by HR-TEM, air tempering, and X-ray diffraction analysis.

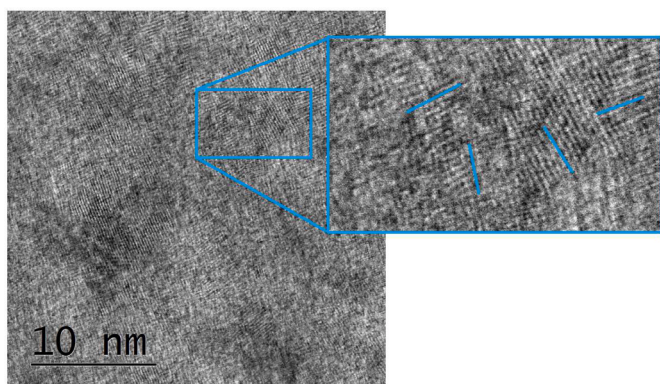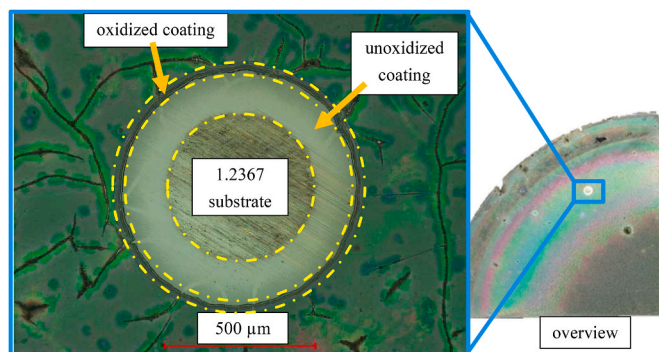The processed images used for the digital image analysis regarding

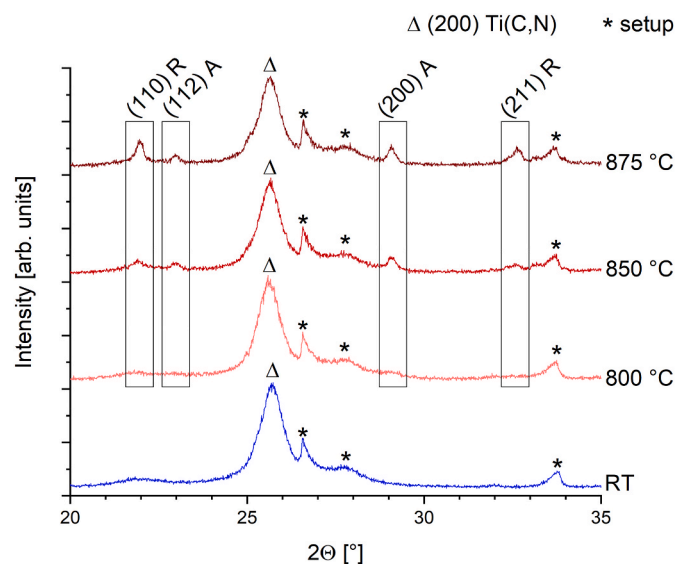**Fig. 5.** Crater in Ti–Si–B–*C*–N that was air annealed made with ballcratering method.

Fig. 6. In-situ X-ray diffraction patterns at elevated temperatures for Ti–Si–B–*C*–N coating. "A" marks anatase and "R" rutile TiO_2 reflexes.

the copper adhesions on the die inserts are shown in Figs. 7 and 8. The inserts' die faces are illustrated in black and adhesions are marked red. Significant decrease in adhesion can be identified by comparing untreated and borided alloy 718. As shown in Fig. 7 a., the untreated die insert is covered on approx. 36 %. In contrast, copper residues adhere to only 5 % of the borided insert's die face (see Fig. 7 b.). Moreover, the adhesions appear merely in the form of thin lines, instead of large-area defects.

Fig. 8 exposes a major difference between the untreated die face (Fig. 8 a.) and the Ti–Si–B–*C*–N coated die face (Fig. 8 b.) considering the inserts made of DIN 1.2367. The area covered with copper is approx. 82 % on the untreated insert, whereas it is only 6 % on the surface-modified insert. Considering the drastically reduced area with adhesions, this proves the effectiveness of the PECVD coating with respect to the reduction of adhesion between copper and hot work steel DIN 1.2367. As with the boriding of alloy 718, this reflects a substantial improvement on the adhesion behavior resulting from Ti–Si–B–*C*–N coating on hot work steel.

4. Conclusions

Hot extrusion of copper was carried out with a two-hole die consisting of a die holder and two separate die inserts. The four inserts were made of DIN 1.2367, plasma nitrided and Ti–Si–B–*C*–N coated DIN 1.2367, alloy 718, and borided alloy 718. A close examination of

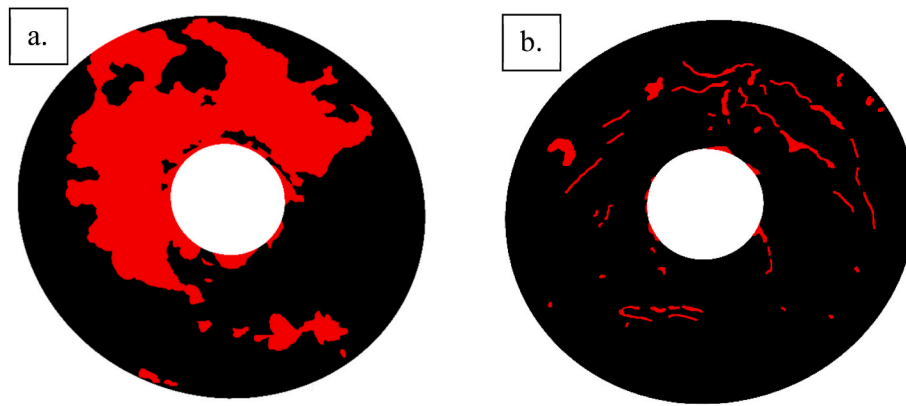**Fig. 4.** HR-TEM image of a Ti–Si–B–*C*–N PECVD coating.

Fig. 7. Digitally processed images of the die inserts made of alloy 718 a. Without surface modification and b. With borided surface. Areas covered with copper adhesions are marked red. (For interpretation of the references to color in this figure legend, the reader is referred to the Web version of this article.)
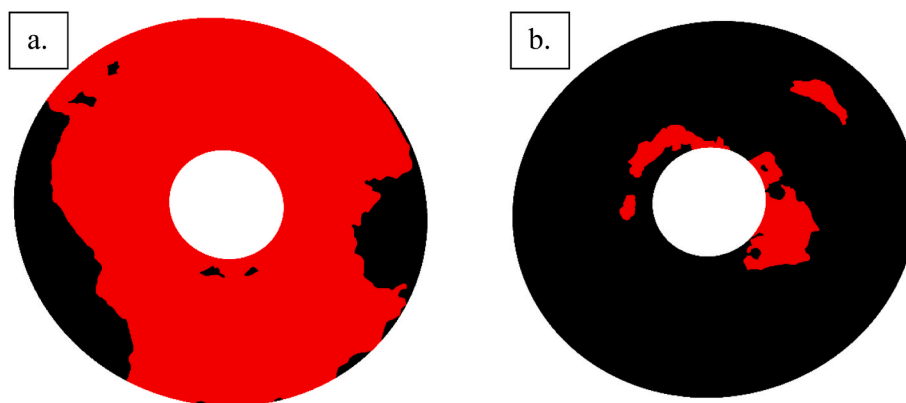

Fig. 8. Digitally processed images of the die inserts made of DIN 1.2367 a. Without surface modification and b. With Ti–Si–B–*C*–N coating. Areas covered with copper adhesions are marked red. (For interpretation of the references to color in this figure legend, the reader is referred to the Web version of this article.)

appearance of the die inserts after extrusion showed significantly lower adhesion of copper in case of both surface modifications. To gain insights on the mechanisms that lead to lower adhesive wear, the surface modifications were characterized experimentally using HR-TEM, X-ray diffraction, cross-sectional investigation, and hardness measurement. Additionally, samples were tempered in air and investigated afterwards to evaluate oxidation resistance. Oxidation resistance of both surface modifications exceed the billet temperature, which is a mandatory asset for this application. The abrasive wear does not contribute to the total wear significantly, but high hardness is nonetheless favorable for wear applications.

In the near future, further investigations will be conducted on a friction tester for extrusion processes, with the aim of quantitatively characterizing the adhesion behavior of the surface modifications. Additionally, the impact of surface roughness will be closer examined, as it plays a significant role in adhesion in hot forming of aluminum, which shows parallels concerning adhesion on tool's surface.

Additional experiments in hot extrusion processes are necessary to fully understand the potential of surface modifications, as all of the extrusion processes were carried out without lubrication to intentionally provoke massive adhesive wear and identify differences between modified and unmodified tool materials. The addition of graphite-based lubricants will presumably lower friction and adhesion between tool and copper, thus reducing wear in the processes even further.

CRediT authorship contribution statement

Alexander Thewes: Conceptualization, Data curation, Formal analysis, Funding acquisition, Investigation, Methodology, Project administration, Resources, Visualization, Writing – original draft. **Phillip Marvin Reinders:** Investigation, Resources, Writing – review & editing. **Hanno Paschke:** Conceptualization, Investigation, Writing – review & editing. **Tristan Brückner:** Conceptualization, Investigation, Writing – review & editing. **Daniel Templin:** Data curation, Investigation, Resources, Writing – review & editing. **Stefan Lechner:** Data curation, Funding acquisition, Investigation, Methodology, Project administration, Writing – original draft, Writing – review & editing. **Sören Müller:** Project administration, Resources, Writing – review & editing. **Michael Paulus:** Data curation, Investigation, Resources, Writing – review & editing. **Christian Sternemann:** Data curation, Investigation, Resources, Writing – review & editing.

Declaration of competing interest

The authors declare that they have no known competing financial interests or personal relationships that could have appeared to influence the work reported in this paper.

Data availability

Data will be made available on request.

Acknowledgement

References

[1] P. Villanueva-Rey, S. Belo, P. Quinteiro, L. Arroja, A.C. Dias, Wiring in the automobile industry: life cycle assessment of an innovative cable solution, J. Clean. Prod. 204 (2018) 237–246, https://doi.org/10.1016/j.jclepro.2018.09.017.

[2] W. Gissler, Structure and properties of Ti-B-N coatings, Surf. Coating. Technol. (1994) 556–563.

[3] P. Karvankova, M. Veprek-Heijmann, D. Azinovic, S. Veprek, Properties of superhard nc-TiN/a-BN and nc-TiN/a-BN/a-TiB2 nanocomposite coatings prepared by plasma induced chemical vapor deposition, Surf. Coating. Technol. (2006) 2978–2989.

[4] S. Veprek, M. Veprek-Heijman, P. Karvankova, J. Prochazka, Different approaches to superhard coatings and nanocomposites, Thin Solid Films 476 (2005) 1–29, https://doi.org/10.1016/j.tsf.2004.10.053.

[5] X. Chen, S. Ma, K. Xu, P.K. Chu, Oxidation behavior of Ti–B–C–N coatings deposited by reactive magnetron sputtering, Vacuum 86 (2012) 1505–1512, https://doi.org/10.1016/j.vacuum.2012.03.001.

[6] H.J. Seifert (Ed.), Refractory and Hard Materials in the Ti-Si-B-C-N System: Phase Equilibria, Phase Reactions and Thermal Stabilities, 2005.

[7] N. Ueda, T. Mizukoshi, K. Demizu, T. Sone, A. Ikenaga, M. Kawamoto, Boriding of nickel ny powder-pack method, Surf. Coating. Technol. (2000) 25–30.

[8] D.C. Lou, J.K. Solberg, O.M. Akselsen, N. Dahl, Microstructure and property investigation of paste boronized pure nickel and Nimonic 90 superalloy, Mater. Chem. Phys. 115 (2009) 239–244, https://doi.org/10.1016/j.matchemphys.2008.11.055.

[9] M. Makuch, M. Kulka, Microstructural characterization and some mechanical properties of gas-borided Inconel 600-alloy, Appl. Surf. Sci. (2014) 1007–1018, https://doi.org/10.1016/j.apsusc.2014.06.109.

[10] M. Makuch, Nanomechanical properties and fracture toughness of hard ceramic layer produced by gas boriding of Inconel 600 alloy, Trans. Nonferrous Metals Soc. China 30 (2020) 428–448, https://doi.org/10.1016/S1003-6326(20)65224-4.

[11] D.-w. Deng, C.-g. Wang, Q.-q. Liu, T.-t. Niu, Effect of standard heat treatment on microstructure and properties of borided Inconel 718, Trans. Nonferrous Metals Soc. China 25 (2015) 437–443, https://doi.org/10.1016/S1003-6326(15)63621-4.

[12] I. Campos-Silva, A.D. Contla-Pacheco, A. Ruiz-Rios, J. Martínez-Trinidad, G. Rodríguez-Castro, A. Meneses-Amador, W.D. Wong-Angel, Effects of scratch tests on the adhesive and cohesive properties of borided Inconel 718 superalloy, Surf. Coating. Technol. 349 (2018) 917–927, https://doi.org/10.1016/j.surfcoat.2018.05.086.

[13] I. Campos-Silva, A.D. Contla-Pacheco, U. Figueroa-López, J. Martínez-Trinidad, A. Garduño-Alva, M. Ortega-Avilés, Sliding wear resistance of nickel boride layers on an Inconel 718 superalloy, Surf. Coating. Technol. 378 (2019) 124862, https://doi.org/10.1016/j.surfcoat.2019.06.099.

[14] A. Nienhaus, G. Braeuer, H. Paschke, D. Stangier, W. Tillmann, M. Paulus, C. Sternemann, Nanocomposite PECVD multiphase coatings for wear reduction under thermal load conditions, in: Proceedings 3. Niedersaechsisches Symposium Materialtechnik, 2019, pp. 511–521, https://doi.org/10.21268/20190320-4.

[15] A. Thewes, L. Bröcker, E.T.K. George, G. Bräuer, M. Paulus, C. Sternemann, H. Paschke, T. Brückner, S. Lechner, S. Müller, Ti-Si-B-C-N plasma enhanced chemical vapor deposition nanocomposite coatings for high temperature applications, Thin Solid Films 760 (2022) 139507, https://doi.org/10.1016/j.tsf.2022.139507.

[16] S. Ma, Y. Li, K. Xu, The composite of nitrided steel of H13 and TiN coatings by plasma duplex treatment and the effect of pre-nitriding, Surf. Coating. Technol. (2001) 116–121. PII: S0257-8972_00.01073-2.

[17] M. Zlatanović, T. Gredić, N. Popović, Ž. Bogdanov, Matching of TiN coating structures by plasma nitriding of substrates, Vacuum 44 (1993) 83–88, https://doi.org/10.1016/0042-207X(93)90353-C.

[18] C. Leroy, K.I. Schiffmann, K. van Acker, J. von Stebut, Ball cratering an efficient tool for 3 body microabrasion of coated systems, Surf. Coating. Technol. 200 (2005) 153–156, https://doi.org/10.1016/j.surfcoat.2005.02.076.

[19] C. Krywka, M. Paulus, C. Sternemann, M. Volmer, A. Remhof, G. Nowak, A. Nefedov, B. Pöter, M. Spiegel, M. Tolan, The new diffractometer for surface X-ray diffraction at beamline BL9 of DELTA, J. Synchrotron Radiat. 13 (2006) 8–13, https://doi.org/10.1107/S0909049505035685.

[20] S. Lechner, A. Thewes, S. Müller, Reduction of friction and adhesion in coppor and brass extrusion by application of boron containing surface modifications, in: TMS 2023 152nd Annual Meeting & Exhibition Supplemental Proceedings, Springer Nature Switzerland, Cham, 2023, https://doi.org/10.1007/978-3-031-22524-6_36.

[21] J. Patscheider, T. Zehnder, M. Diserens, Structure–performance relations in nanocomposite coatings, Surf. Coating. Technol. 146–147 (2001) 201–208, https://doi.org/10.1016/S0257-8972(01)01389-5.

[22] D. Pilloud, J.F. Pierson, M.C. Marco de Lucas, A. Cavaleiro, Study of the structural changes induced by air oxidation in Ti–Si–N hard coatings, Surf. Coating. Technol. 202 (2008) 2413–2417, https://doi.org/10.1016/j.surfcoat.2007.09.017.

[23] P.H. Mayrhofer, C. Mitterer, J.E. Greene, Thermally induced self-hardening of nanocrystalline Ti-B-N thin films, J. Appl. Phys. 100 (2006) 044301-1–044301-7, https://doi.org/10.1063/1.2222406.